Connectomic Analysis of the *Drosophila* Lateral Neuron Clock Cells Reveals the Synaptic Basis of Functional Pacemaker Classes

Shafer, O.T.[1,*], Gutierrez G.J.[2,*], Li, K.[3], Mildenhall, A.[3], Spira, D.[2,3], Marty, J.[4], Lazar, A.A.[4], and Fernandez M.P.[3,#]

1- Advanced Science Research Center, Graduate Center, The City University of New York. New York, NY 10031
2- Center for Theoretical Neuroscience, Zuckerman Institute, Columbia University. New York, NY 10027
3- Department of Neuroscience and Behavior, Barnard College. New York, NY 10027
4- Department of Electrical Engineering, Columbia University. New York, NY 10027

*Equal contribution
#Correspondence should be submitted to Maria Paz Fernandez (mfernand@barnard.edu)

Abstract

The circadian clock orchestrates daily changes in physiology and behavior to ensure internal temporal order and optimal timing across the day. In animals, a central brain clock orchestrates circadian rhythms throughout the body and is characterized by a remarkable resilience that depends on synaptic connections between constituent neurons. The clock neuron network of *Drosophila*, which is built of many fewer neurons yet shares network motifs with clock networks in the mammalian brain, offers a powerful model for understanding the network properties of circadian timekeeping. Here we report an assessment of synaptic connectivity within a clock network, focusing on the critical LN clock neuron classes. Our results reveal that previously identified anatomical and functional subclasses of LNs represent distinct connectomic types with distinct synaptic output pathways. Moreover, we identify a small number of clock cell subtypes representing highly synaptically coupled nodes within the fly's clock neuron network, and suggest that neurons lacking molecular timekeeping likely play integral roles within the circadian timekeeping network. To our knowledge, this represents the first comprehensive connectomic analysis of a neural network capable of driving endogenous circadian rhythms. The

organizational principles uncovered in this study provide remarkable insights into clock network organization.

Introduction

Most organisms undergo predictable daily changes in gene expression, physiology, and behavior that are driven by endogenous circadian clocks (1, 2) . In animals, the molecular feedback loops underlying circadian clocks are present in all organ systems but are required within a relatively circumscribed population of brain neurons for the maintenance of daily rhythms in behavior and physiology (3). In mammals, the hypothalamic suprachiasmatic nuclei (SCN) represent the brain's central circadian clock: the ablation of the SCN or knockouts of the molecular clock within it result in a loss of circadian rhythms (reviewed by (4)). Compared to molecular timekeeping in peripheral tissues, timekeeping in the brain's central clock is more resilient to the loss of clock gene function or to environmental perturbations, a resilience afforded by physiological connections between its constituent neurons (5, 6). Determining how clock networks are structured with regard to neural connectivity is therefore essential if we are to understand circadian timekeeping in animals.

A fundamental challenge to addressing this question is the complexity of the neural networks mediating circadian timekeeping. The paired mammalian SCN consist of tens of thousands of neurons that employ a great diversity of neurochemical outputs and form a complex and highly interconnected network (reviewed by (7)). The clock neuron network of *Drosophila melanogaster* offers a powerful model for the network properties of neural circadian timekeeping. The molecular clocks of insects and mammals are highly conserved and their neural networks appear to share common motifs, yet the fly's clock neuron network offers a numerical simplicity that is of great utility to the experimentalist (8). The fly's clock neuron

network consists of relatively few neurons (~75 per brain hemisphere) that can be organized into a small number of discrete anatomical classes ((9); Figure 1A). Furthermore, genetic tools for the specific manipulation of anatomical subclasses of the fly have made it possible to characterize the functional roles of these subclasses in the production of endogenous circadian rhythms in sleep and activity (10, 11). Though transgenic markers of synaptic connectivity and live-imaging-based assessments of functional connectivity have been used to address neural connectivity within the clock neuron network (e.g., (12, 13), a systematic accounting of synaptic connectivity within this network is lacking. Such an accounting would provide valuable insights into the network structure of neural circadian timekeeping in the brain.

The comprehensive mapping of synaptic connectivity using serial electron microscopy and reconstruction of neuronal volumes allows for an unprecedented ability to directly assess network structures of brain circuitry (14). Scheffer and colleagues (15) have provided a dense reconstruction of chemical synapses within a large portion of the fly's central brain, a volume called the hemibrain. Furthermore, the annotation of the hemibrain connectome contains the majority of the key anatomical subsets of the fly's clock neuron network and powerful computational tools are available for navigating this connectome (15, 16) making possible an assessment of the general network structure of the fly's brain clock.

The current annotation of the hemibrain data set identifies all the expected lateral neuron (LN) classes: four l-LNvs, four s-LNvs, the 5th-s-LNv, and six LNds ((15); Figure 1B and C). In addition, all of the LPN and DN1as have been identified, as have seven out of the ~15 expected DN1ps (13, 15). However, some clock neurons have not yet been unequivocally identified within the hemibrain data set: approximately half of the DN1ps and all of the DN2s and DN3s. The LN classes of clock neuron represent the minimum sub-network required for the production of the endogenous bimodal rhythm of sleep and activity; functional molecular circadian timekeeping

only in the s-LNvs, 5th-s-LNv, and LNds is sufficient for the production of such rhythms (17, 18). As described below, much of the synaptic connectivity displayed by the l-LNvs likely occurs outside of the hemibrain volume. We have therefore largely omitted the l-LNvs from our analysis.

Here we report an assessment of chemical synaptic connectivity for the critical LN clock neuron classes within the hemibrain volume, thereby determining the patterns of synaptic connectivity between this core circadian sub-network, their synaptic inputs and outputs, and their patterns of connectivity with other clock neurons annotated within the hemibrain dataset. This analysis provides significant insight into the organization and function of the *Drosophila* central brain clock. Our results reveal that previously identified anatomical and functional subclasses of LN represent distinct connectomic classes, receiving unique sources of synaptic inputs and outputs and implicating specific, identified neurons as important nodes for circadian entrainment and output. Our results also suggest a significant revision in the longstanding anatomical classification of the LNs. Furthermore, our analysis reveals a remarkable heterogeneity in the extent to which clock neuron subclasses form connections to other clock neuron classes and identifies a small number of clock cell subtypes representing highly synaptically coupled nodes within the fly's clock neuron network. Finally, we reveal "non-clock neuron" targets who themselves form synapses back onto the clock neuron network, suggesting that timekeeping networks likely contain neurons not previously recognized as part of the core clock network due to the absence of clock gene expression.

Results

The Clock Neuron Network and the Hemibrain Dataset

Representatives of all classes of clock neurons, with the exception of the DN2 and DN3 classes, are identified in the annotation of the hemibrain volume used here (Figure 1A and B; please see Table 1 for the naming scheme used here for the clock neurons identified in the dataset with their corresponding unique body IDs). The patterns of connectivity among some of these neurons have recently been briefly described (11, 13). Scheffer and colleagues (15) define synaptic strength within the hemibrain volume based on the number of synaptic connections formed between neurons, defining connections consisting of only one or two chemical synapses as weak and subject to error, three to nine synapses as medium strength, and of ten or more synapses as strong. We employ these definitions of synaptic strength throughout this study. When taken as a whole, the identified clock neurons appear to be sparsely interconnected by chemical synapses. The majority of clock neuron pairs form either no synapses or weak synaptic connections (Figure 1C). However, there are a few clear exceptions: a single LNd (LNd6) and the 5th s-LNv form strong connections with one another and with members of the DN1 group (Figure 1C; see also Reinhard and colleagues (13)). LNd6 and the 5th s-LNv stand out among the identified clock neurons as particularly rich hubs of inter-clock synaptic connectivity.

To begin an assessment of the patterns of synaptic connectivity displayed by the clock neuron network of *Drosophila*, we have focused on three critical classes of lateral clock neuron; the Pigment Dispersing Factor (PDF) -expressing small ventral lateral neurons (s-LNvs), the dorsal lateral neurons (LNds) and the PDF negative 5th s-LNv (Figure 1D). We have chosen to focus on these clock neuron classes for two reasons. First, these classes are completely accounted for in the hemibrain annotation used here. Second, the LN classes alone are sufficient to drive the fly's endogenous bimodal rhythm in locomotor activity (17, 18) and therefore appear to be a critical sub-network within the fly's circadian system.

The small LN_vs are a highly unified connectomic class distinct from the 5th s-LNv.

The s-LNvs have long been considered critical circadian pacemakers within the *Drosophila* clock neuron network (19). Like the l-LNvs, the s-LNvs express the neuropeptide PDF (20, 21), but unlike the l-LNvs they maintain strong molecular timekeeping under constant conditions (22, 23) and are required for robust endogenous circadian rhythms (17, 24). The s-LNvs also contribute significantly to the morning peak of the fly's crepuscular daily activity rhythm (17, 25). Though by no means the only clock neurons capable of producing an endogenous sense of time (26-28), a large body of evidence supports the contention that s-LNvs are among the most critical neurons for the maintenance of endogenous circadian rhythms (Reviewed by (11)). The 5th-s-LNvs, though they do not express PDF, were named based on their apparent anatomical similarity to the PDF positive s-LNvs in the larval brain (18, 29). However, subsequent work has suggested that the 5th s-LNv is likely functionally and anatomically more akin to the LNds (17, 26, 30).

The PDF-expressing s-LN_vs are characterized by a relatively simple morphology (Figure 2A; (31)). Their cell bodies are located in the ventral brain, near the accessory medulla (AMe), into which they extend short neurites which are thought to receive input from external photoreceptors (32, 33). These s-LNvs project dorsally to the posterior dorsal protocerebrum, where they turn toward the midline and form fine ramified termini that extend toward the midline (31, 34). These dorsal ramifications are thought to be the major site of s-LNv synaptic output, but are also known to contain synaptic inputs (35). Work by Schubert and colleagues (30) shows that the 5th s-LNv (Fig 2F) is characterized by more extensive ramifications within the dorsal brain and accessory medulla compared to the PDF expressing s-LNvs.

All four PDF-expressing s-LNvs have been identified within the hemibrain data set, as has the 5th s-LNv (Figures 1B-C and Figure 2A,F; (15)). Visualization of T-bars and postsynaptic densities within these neurons reveals that their ventral neurites, which innervate the AMe, are heavily biased toward synaptic input (Figure 2A and F). Individual PDF-positive s-LNvs display relatively simple dorsal medial termini with relatively few branch-points that tend to run in parallel to neighboring branches (Supplemental Figure 1). As previously described (35), these dorsal medial s-LNv termini contain both presynaptic and postsynaptic structures with the former significantly outnumbering the latter (Figure 2A and Supplemental Figure 1). The dorsal termini of the 5th s-LNvs also contains both pre- and post-synaptic structures, but compared to PDF expressing s-LNvs, appear to be less biased toward output (Fig. 2F). Taken together, the PDF-positive s-LNvs within the hemibrain volume contain a total of 505 postsynaptic densities and project onto a total of 1733 postsynaptic densities on post-synaptic neurons. Remarkably, the single 5th s-LNv contains 1413 post-synaptic densities and forms synapses onto 1992 postsynaptic densities. Thus, the 5th s-LNv forms about four times the number of synapses of a single PDF-positive s-LNv (Figure 4C; Supplemental Table S1 and S2).

With regard to strong synaptic connections, the s-LNvs display remarkable uniformity in their synaptic inputs. Only three neurons within the hemibrain provide ten or more synapses onto at least one of the four s-LNv (Figure 2D), and all four s-LNvs receive strong or medium strength synaptic inputs from these three presynaptic cell types (Figure 4D; Supplemental Table S1). The s-LNvs also appear to be remarkably uniform in their patterns of strong synaptic output. Only 11 neurons receive 10 or more synapses from at least one s-LNv (Figure 2E and 4E), and all 11 receive strong or medium strength synapses from all four s-LNvs (Figure 4E; Supplemental Table S2). Compared to the other LN classes, the s-LNvs are highly unified in both their strong and medium strength connections (Figure 4A and B) and form few but nearly uniform patterns of strong synaptic connections (Figure 4C and D). Remarkably, within the

hemibrain volume, identified clock neurons are not among the cell types that are strongly connected to the s-LNvs, which form very few synapses on other identified clock neurons (3% of output and ~12% of input synapses; Figure 1C), though the s-LN$_v$s do form medium strength connections with one another (Figures 1C and 2H). The 5th s-LNv displays patterns of strong synaptic connectivity that are almost completely distinct from those of the PDF-positive s-LNvs, sharing a single strong output connection with only one of these cells (Figure 2E).

Though quite uniform in their patterns of strong synaptic input and outputs, the s-LNvs do display some within-class differences in their patterns of weak and medium strength connections. Among the inputs targeting only one s-LNv, and mediated by only three synapses, is the HB-eyelet, a surprising finding given the long-held model that this external photoreceptor provides direct excitatory input onto s-LN$_v$s and contributes to light entrainment of circadian rhythms (32, 33, 36), though recent work has indicated that the eyelet to s-LNv connection may be polysynaptic (37). Nevertheless, our analysis supports the notion that, with regard to patterns of strong synaptic connections, the s-LN$_v$s represent a uniform connectomic cell type, consistent with recent work revealing a uniformity in gene expression across the s-LNvs (38).

The LNds comprise several connectomic subclasses.

As their name suggests, the somata of the dorsal lateral neurons (LNds) are situated dorsally relative to the LNvs, residing in the lateral cell body rind (29-31). All six of the LNds send dorsal medial projections across the superior protocerebrum and three of the six send an additional projection toward the ventral brain ((30); Figure 3A and Supplemental Figure S2). Though consisting of only two more neurons than the PDF-positive s-LNv class, the LNds form seven-times more synaptic connections (6149 postsynaptic densities and projections to 9590 PSDs; compare Figures 2A, 3A, and 4C) and are characterized by a much larger number of strong

synaptic partners. There are 164 distinct neurons that receive strong synaptic inputs from at least one LNd (compared to 11 neurons for s-LNvs; (Supplemental Table S2), and 86 distinct neurons provide strong synaptic input onto at least one LNd (compared to three for s-LNvs; Supplemental Table S2).

In addition to forming more synapses with more neurons than the PDF-positive s-LNvs, the LNds are markedly less uniform in their patterns of strong synaptic connections (Figures 3E and F and 4F and G). There is not a single source of strong synaptic input or a single neural target of synaptic output that forms strong connections with all six LNds (Figure 3E and F, Supplemental Tables S1 and S2). The maximum number of LNds that receive strong synaptic inputs from the same presynaptic neuron is three (Figure 3F). The maximum number of LNds that form strong synaptic outputs onto the same neuronal targets is also three (Figure 3F). Based on these patterns of shared strong connectivity, there appears to be two general connectomic groups within the LNds, each consisting of three neurons: LNds 1-3 and LNds 4-6. LNds within these two subgroups are more similar in their patterns of strong synaptic connectivity to each other than to LNds of the other group (Figure 3E and F and 4F and G). These two groups differ to a remarkable degree in the number of their synaptic connections, with the LNd 4-6 group forming approximately twice the number of synaptic connections (Figure 4C; Supplemental Figure S2 and Supplemental Tables S1 and S2).

An examination of the cellular morphology of the LNds within the hemibrain volume reveals that LNds 4-6 extend both dorsal-medial and ventral projections, whereas LNds 1-3 extend only dorsal-medial projections (Supplemental Figure S2). As previously shown by Schubert and colleagues (30), this indicates that LNds 4-6 correspond to the Cryptochrome (Cry) expressing LNds, while LNds 1-3 correspond to the Cry negative LNds. Though the Cry+ and Cry- subgroups of the LNds appear to represent two distinct connectomic subtypes, patterns of

strong synaptic connectivity suggest that the LNds can be further divided based on their patterns of strong synaptic connections. Within the Cry+ LNds, LNd4 and LNd5 share 27 strong synaptic inputs with one another, but only seven strong connections with LNd6 (Figure 3E), while sharing 33 strong synaptic targets with one another but only seven or fewer with LNd6 (Figure 3F). Thus, the Cry+ LNds appear to consist of at least two connectomic subgroups, LNd4/LNd5 and LNd6. This connectomic distinction is consistent with differences in neuropeptide expression within the Cry+ LNds, with two LNds expressing short neuropeptide F (sNPF) and the third expressing ion transport peptide (ITP), a feature it shares with the Cry expressing 5th s-LNv (39). A similar distinction can be made for LNd2/LNd3 and LNd1 with regard to patterns of strong synaptic connections by the Cry- LNds (Figure 3E and F). Based on these patterns of strong synaptic connections, the LNd class appears to consist of four distinct connectomic types, a number that matches precisely the number of transcriptomic classes of LNds recently revealed by single cell sequencing methods (38).

The four connectomic groups of LNd clock neurons conform to previously identified cellular and functional clock subsets.

In addition to differences in Cry expression, the LNds display other cellular and functional distinctions, suggesting that this clock neuron class consists of multiple neuronal subtypes. The LNds are divisible based on their expression of neuropeptides and neurotransmitters (39), with two LNds co-expressing sNPF and Choline acetyltransferase (ChAT), an enzyme involved in the biosynthesis of acetylcholine. Three LNds express Neuropeptide F (NPF), one of which expresses a second peptide, ITP (39). The transmitter(s) produced by the remaining LNd are not currently known. Furthermore, Cry+ and Cry- LNds differ in their expression of Pdf receptor (PdfR), with the Cry+ LNds uniformly expressing PdfR and the Cry- LNds lacking receptor

expression (40), suggesting that these two groups of LNd are differentially sensitive to PDF released from the l-LN_vs and s-LN_vs.

The coupling of LNds to circadian timekeeping within the s-LNvs varies among the LNds. The two sNPF positive LNds, which express Cry and PdfR, remain tightly coupled to the s-LNvs when the circadian clock in the latter neurons is slowed down (26). The sNPF expressing LNds were termed E1 oscillators based on this tight temporal coupling to the s-LNvs (26), which also express sNPF (39). The NPF/ITP expressing LNd, despite being receptive to PDF released from the LNvs, does not display coupling to the slowed s-LNv clocks and were grouped with the ITP-expressing 5th s-LNv as E2 oscillators (26). The remaining LNds, which consist of the Cry negative LNds, were classified as E3 oscillators, which are neither PDF receptive nor coupled to s-LNvs with modified clock speeds (26).

The Cry+ LNds therefore appear to consist of two functional types; two LNds making up E1 and a single LNd corresponding to E2. Schubert and colleagues (30) established the anatomical hallmarks of these two Cry+ LNds, with the single E2 LNd sending more extensive ventral projections compared to the E1 LNds. Examination of hemibrain LNd volumes indicates that LNd6 corresponds to LNd-E2 (compare Supplemental Figure S2D and E to F), revealing that LNd4 and LNd5 correspond to the E1 LNds. This LNd5/4 (E1) and LNd6 (E2) distinction mirrors the patterns of shared strong synaptic connectivity displayed by the Cry+ LNds (Figure 3E and F). Therefore, functionally distinct LNd subgroups appear also to be connectomically distinct with regard to strong synaptic inputs and outputs.

The 5th s-LNv, which shares cellular and anatomical similarities with LNd6 (30, 39), was assigned as a member of the E2 functional class by Yao and Shafer (26), based on the absence of coupling to timekeeping within the PDF positive s-LNvs, despite receptivity to PDF and their

role in the generation of evening activity (17). We therefore asked if LNd6 and the 5th s-LNv display similar patterns of synaptic connectivity. Indeed, these two neurons displayed significant overlap in their strong synaptic connectivity, both for synaptic inputs and targets (Figure 4F and G). Thus, in addition to sharing neuropeptide expression and coupling mode with the PDF expressing s-LNvs (26), LNd6 and the 5th s-LNv are more alike in their patterns of strong synaptic connectivity than they are to other lateral neuron subtypes.

The patterns of strong clock neuron connectivity within the hemibrain led us to hypothesize that the recognized functional subtypes, M (PDF positive s-LNvs), E1 (LNd4 and LNd5), E2 (LNd6 and 5th s-LNv), and E3 (LNd1, LNd2, and LNd3) display distinct patterns of synaptic connectivity. To challenge this hypothesis, we expanded our analysis to include both strong and medium strength synaptic connections, which together account for the vast majority of connections made by the identified clock neurons within the hemibrain dataset. To examine affinities between individual identified clock neurons in our expanded consideration of connectivity, we made use of the Jaccard index (Fig 4A and B), a coefficient of similarity between two sets that ranges between zero and one, the former value indicating no overlapping synaptic partners and latter indicating complete overlap (see methods). Jaccard indices for both synaptic inputs (Fig 4A) and outputs (Fig 4B) provide strong evidence that the LN classes can be divided into four connectomic groups: The four PDF positive s-LNvs (M group; Figure 6), two of the Cry+ LNds (LNd4 and LNd5; E1 group; Figure 7), LNd6 and the 5th s-LNv (E2 group; Figure 8 and Supplemental Figure S3), and the Cry- LNds (LNd1, LNd2, and LNd3; E3 Group; Figure 9), conforming to the functional divisions first hypothesized by Yao and Shafer (26).

These functional LN divisions also are distinctive with regard to the number of synaptic connections they make and the ratios of input to output synapses. The M group displays the smallest number of synapses, E3 an intermediate number, and E1 and E2 form roughly twice

the number of connections displayed by E3 (Figure 4C). The M and E1 groups also appear to be distinct from the E2 and E3 groups in the balance of output to input synapses. Though all the identified LNs form more synaptic outputs than inputs, output synapses in the M and E1 groups make up a larger proportion of total synaptic connections when compared to the E2 and E3 groups (Figure 4). Thus, the connectomic subgroups that emerged from our analysis of strong synaptic connectivity (Figures 2-4) are further supported by the combined analysis of strong and medium strength connectivity and conform to previously hypothesized functional and cellular subgroups.

The Functional/Connectomic Subgroups of LN Clock Cells Display Distinct Synaptic Output Pathways

In animals, the brain's endogenous central circadian clock drives myriad behavioral, physiological, and endocrine rhythms, and synaptic connections between the central clock network and neurons outside the timekeeping network are thought to mediate daily signals from the circadian system to the neural centers responsible for driving daily physiological and behavioral changes. Though specific output pathways linking the clock to specific endocrine and sleep control centers have been previously described in the fly (Reviewed by (10, 41)), there is still a great deal to be learned regarding the neural mechanisms underlying circadian output signaling. For example, do the various functional groups of clock neurons converge on the same synaptic targets to shape the timing of the same daily outputs, as was recently described for arousal promoting pathways linking the LNs to dopaminergic neurons modulating the fan-shaped body (42)? Alternatively, do functional clock cell subgroups generally synapse onto distinct neural targets to produce uniquely phased outputs of different behavioral, physiological, and endocrine rhythms, as recently described for sleep modulating dorsal clock neurons (43,

44)? We examined the patterns of synaptic outputs of the LN oscillator subgroups to determine how they might coordinate the myriad outputs of the circadian system.

As previously described (30) M, E1, E2, and E3 subgroups can be distinguished by their patterns of neuropil innervation. As expected, the M, E1, E2, and E3 subgroups differ significantly with regard to where the majority of their neurites form chemical synapses. Though the M and E subgroups form output synapses within both the superior lateral protocerebrum (SLP) and superior medial protocerebrum (SMP), the M subgroups form the majority of their output synapses within the SLP, whereas the E groups form the majority of their output synapses within the SMP (Figure 5A and B). Though all seven E cells terminate largely within these two neuropils, they fall, once again, into three classes with regard to their neuropil innervation. For example, among the E subgroups E1 forms more output synapses on cells of the anterior ventrolateral protocerebrum (AVLP) than E2 or E3, E2 forms more synapses within the accessory medulla (aMe) than do E1 or E3, and E3 forms little to no synapses on neurons associated with either of these neuropils (Figure 5B).

The M subgroup's shared strong synaptic outputs represent only three distinct cell types (Figure 6). Among these are five neurons within the SLP, which represent only two cell-types: three neurons defined within the annotation as SLP-316-R (Figure 6A) and two neurons defined as SLP-403-R (Figure 6B). The sixth strong shared output is an SMP-associated neuron defined as SMP232-R (Figure 6C). The SLP-316-R neurons bear a remarkable resemblance to DN1ps currently missing from the hemibrain annotation, which send ventral projections alongside the dorsal projections of M cells and named ventral-contralateral DN1ps by Lamaze and colleagues (44), though in this case they do not appear to cross the midline as would be expected of this clock cell type (Figure 6A and Supplemental Figure S10). Jaccard indices support the conclusion that these strong shared targets of M output represent three distinct cell types

(Figure 6D). Remarkably, all of the shared strong output targets of the M group form synapses onto identified clock neurons (Figure 6A-C), including strong synaptic connections onto DN1ps and LPNs (Figure 6E). Thus, all the strong and shared output targets of the M group recur back to the clock neuron network, thereby implicating them as nodes within the clock neuron network, either as currently unidentified clock-containing neurons or non-clock-containing neurons situated within the timekeeping network. The M group appears to be unique in the extent to which its strong shared synaptic targets reenter the clock neuron network, with only half or fewer of strong E1, E2, or E3 targets recurring to the clock network in this fashion (Figure 6F).

The E1 subgroup is characterized by many more strong/shared synaptic targets than the M subgroup (Compare Figure 4E and G) and these targets appear, based on Jaccard indices, to include many distinct cell types (Figure 7D). A minority of these E1 targets (16 out of 38) form output synapses onto identified clock neurons within the hemibrain volume. Thus, the majority of the strong shared synaptic outputs of E1 do not immediately recur back to the clock neuron network, in contrast to the uniform recurrence of strong shared M targets to the clock network (Figure 6A-E). Several of the targets receiving the strongest E1 synaptic input do form strong synaptic connections onto clock neurons, particularly back onto the E1 LNds themselves, in addition to LPNs and DN1as (Figure 7E). Notably, the strong shared targets that recur to the clock neuron network, do not display the anatomical hallmarks of any of the currently unannotated clock neurons in the hemibrain data set (e.g., Figure 7A-C). It therefore appears likely that neurons that do not themselves express the molecular circadian clock might nevertheless reside within the central timekeeping network and mediate polysynaptic connections between clock neurons.

The E2 subgroup, like E1, forms strong shared synapses on a much larger number of neuronal targets than the M group (Compare Figure 4E and G) and these targets represent a diverse

array of cell types. Approximately half (14 out of 26) of the strong and shared E2 targets form synaptic connections onto identified clock neurons within the hemibrain (Figure 6F and 8A-C and E). Compared to the recurrent E1 clock connections, E2 forms synapses on identified clock neurons more broadly, forming connections with all currently identified clock neuron classes in the hemibrain volume, with the exception of the DN1a class (Figure 8E). Thus, the E2 group appears not only to represent a hub of strong direct inter-connectivity between identified clock neuron classes (Figure 1C), but also provides additional synaptic clock network inputs via their strong and shared synaptic targets (Figure 8E). As for E1, strong shared targets of E2 recurring to the clock network include neurons that do not share obvious anatomical affinity for currently unidentified clock neurons within the hemibrain dataset (e.g., Figure 8A-C). This suggests, once again, that the circadian timekeeping network of *Drosophila* likely includes neurons that do not themselves support the expression and cycling of the molecular circadian clock.

Compared to the E1 and E2 groups, E3 forms approximately half the number of synaptic connections (Figure 4C and G). With regard to its shared strong outputs, the E3 subgroup forms strong shared synaptic connections onto only 16 neurons (Figure 3F and 4G), five of which form synapses onto identified clock neurons within the hemibrain (Figure 9E). E3 outputs onto clock neurons are limited to LNds and LPNs with most connections forming back onto E3 LNds themselves (Figure 9A-C and E). This makes E3 reminiscent in some ways to the E1 group in that they are characterized by strong shared output targets that form synapses directly back onto their E3 inputs (Figure 7E and Figure 9E). Once again, the strong and shared output targets recurring to the clock network do not bear the anatomical hallmarks of clock neurons missing from the annotation (Figure 9A-C).

Taken together, our analysis indicates that the strong synaptic outputs of the four functional/connectomic LN subgroups, M, E1, E2, and E3, diverge onto distinct neural targets

(Figure 4). Furthermore, many of these synaptic targets synapse back onto neurons within the clock neuron network, including all of the shared and strong output targets of the M subgroup. In contrast, approximately half of the synaptic targets of synaptic output from the E subgroups do not immediately recur to the clock network (Figure 6F). Not only does this implicate specific neuronal targets as conduits of circadian output, it also suggests that neurons not previously identified as “clock neurons" likely represent integral nodes within the neural network from which endogenous circadian timekeeping emerges (see discussion).

Discussion

The Clock Neuron Network within the Hemibrain Volume

Before discussing our connectomic analysis of the LN clock neuron classes, it is important to acknowledge the limitations of the dataset with regard to the clock network as a whole. The hemibrain represents a single hemisphere of the central brain and therefore does not contain the totality of connections from the clock neuron cell bodies it contains. Given that the clock neuron network is highly likely to contain connections between contralateral neurons including clock neurons (45), our estimates of inter-clock connectivity will therefore not include these contralateral connections. Furthermore, recent work suggests that electrical synapses within the clock neuron network likely contribute to circadian timekeeping, (46), but such synapses are not visible in the hemibrain data set (15). Thus, our analysis must necessarily provide an underestimation of connectivity. In addition, clock neuron classes undergo pronounced daily morphological changes that are most likely accompanied by changes in the number and locations of synaptic connections (47-49). Thus, the hemibrain represents but one point, corresponding to the early day (15), within a cycle of changing synaptic connections. Finally,

the hemibrain data set represents a single female fly, whereas the vast majority of experiments on the neural basis of circadian timekeeping have employed male files, thus unexpected patterns of connectivity may represent differences between the well-characterized clock neuron network of males and the less well-studied female network.

Though we are focusing our analysis on the LN clock neuron classes, we have omitted the l-LNvs. We have done so because the synaptic outputs of the l-LNvs are thought to occur in the contralateral accessory medulla (AMe) and much of their synaptic inputs are thought to located in regions of the medulla that are not included in the hemibrain volume (45). We note, in this context, that the l-LNvs do not appear to make significant contributions to endogenous circadian timekeeping (22-24), which is the phenomenon we seek to illuminate here. Despite these limitations, the organizational principles uncovered in this study provide remarkable insights into clock network organization and are sure to generate a significant number of testable hypotheses regarding network function (see below).

Connectomic Classes of LN Clock Neuron Mirror Previously Proposed Functional and Molecular LN Sub-Groups

The lateral neuron classes have long been considered to be critical for the maintenance of endogenous circadian rhythms (19, 21). An examination of genetic mosaics suggested that, within the LNs, the PDF expressing LNvs were responsible for driving the morning peak of daily activity, whereas PDF negative LNds and 5th s-LNv were responsible for driving the evening peak, leading to the designation of the former neurons as “Morning (M) Cells” and the latter as “Evening (E) Cells” (17, 25). Though named based on its anatomical similarity to the other LNv clock neurons in the larval brain (18, 29), there are now numerous observations suggesting that the 5th-s-LNv is functionally and anatomically distinct from the PDF expressing s-LNvs in the

adult brain: the latter neurons are functionally associated with morning activity whereas the former cell type is associated with evening activity (17). Furthermore the 5th s-LNv shares connectivity patterns, neuropeptide expression, and features of cellular anatomy with one of the Cry-expressing LNds (26, 39). Our connectomic analysis further supports the conclusion that the 5th s-LNv is an LNd-like clock neuron that bears little resemblance, functionally or anatomically, to the PDF expressing s-LNvs.

Functional and anatomical analysis suggests that the LN neurons can be divided into four functional classes, M, E1, E2, and E3 and that the patterns of strong connectivity displayed by the LNs are in striking concordance with these divisions (26). Our connectomic analysis indicates that the functional differences characterizing these four groups of neurons appear to be written in the connectome: each receives a unique combination of strong synaptic inputs and, in turn, forms strong synaptic connections onto distinct post-synaptic targets. These results suggest that the functional subsets of LNs likely drive distinct behavioral and physiological outputs, rather than converging onto the same premotor, sleep, or endocrine centers.

In addition, our analysis supports the existence of an additional subgroup within the LNs, suggesting that the Cry- negative E3 class likely consists of two subgroups: LNd2 and LNd3, which share a large proportion of their strong synaptic inputs and outputs, and LNd1, which shares significantly fewer strong connections with the other two Cry- LNds (Figure 3E and F). Placing LNd1 into its own LNd subgroup would align our connectomic LN divisions with a recent transcriptomic analysis of the clock neuron network that divided the LNds into four clusters: The two sNPF and Cry expressing LNds (LNd4 and LNd5, i.e., E1), the single ITP and Cry expressing LNd (LNd6, i.e. the E2 LNd), two NPF expressing LNds lacking Cry expression, and a single Cry- LNd that lacks NPF (38).

The M group forms very few synaptic connections with other identified clock neuron classes in the hemibrain dataset.

The s-LNvs of the M group, though they form medium strength connections with one another, are almost completely synaptically isolated from the other identified clock neurons within the hemibrain dataset (Figure 1C and 2H). Though this picture may ultimately prove an underestimation of inter-clock connectivity if the strong shared SLP targets of M output (Figure 6A) are determined to be the DN1ps currently missing from the annotation (Supplemental Figure S7). The predicted synaptic inputs to the M group from the DN1ps (50-52) are not apparent in the hemibrain dataset, though this may, again, be a limitation of the current annotation in which approximately half of the DN1ps are unaccounted for. However, strong DN1p to s-LNv connections are lacking even if we consider the three strong M cell targets, the SLP316s, to be missing DN1ps, as these form synapses on DN1ps and LPNs, but not the M group (Supplemental Figure S7). Remarkably, there are no synaptic connections between the M and E1 groups, the latter of which was differentiated from E2 by the tight coupling of E1 molecular clocks to those of the M group (26). Thus, the strong coupling of M and E1 likely takes place through non-synaptic connections, consistent with recent work suggesting that the M group mediates its influence over endogenous timekeeping via non-synaptic signaling mechanisms, most likely via the non-synaptic release of PDF peptide (35, 47).

Compared to the other LN subgroups, the M group forms the smallest number of synaptic connections (Figure 4C). It is also unique among the LN groups by virtue of the fact that all of its shared strong synaptic output targets form strong synaptic connections onto neurons within the clock neuron network, forming strong connections onto DN1ps and LPNs (Figure 6E). Thus, the strongest synaptic outputs of the M groups appear to be intimately associated with the clock

neuron network, either as neurons directly linking different clock neuron classes, or as currently unidentified clock neurons within the hemibrain data set (see Supplemental Figure S7).

The E1 and E2 groups are major conduits of synaptic output from the clock network.

Compared to the other three LN functional groups, the E1 group forms the largest number of connections onto post-synaptic neurons (Figures 3F and 4C) and the majority of their strong and shared synaptic targets do not themselves form synapses onto identified clock neurons within the hemibrain data set. Of the minority of strong shared E1 targets that do synapse onto identified clock neurons, the majority form strong reciprocal connections with E1 itself (Figure 7E and 10A). Thus, the E group most strongly coupled with the critical M group (26) also appears to be a major conduit of synaptic output from the clock neuron network.

Among the identified clock neurons within the hemibrain dataset, the E2 LNs (LNd6 and the 5th s-LNv) are clear outliers with regard to synaptic connectivity with other clock neurons, forming strong synaptic connections onto E1 LNds and DN1ps. E2 LNds also receive strong synaptic inputs from DN1as and DN1ps and form strong connections with one another (Figure 1C). This strong synaptic connectivity with other clock neurons may provide an explanation for the observation that the E2 group fails to synchronize its molecular clock with the M group when the clocks of the latter cells are slowed down, despite expressing the receptor for the M group's major circadian output peptide PDF (26). Synaptic communication from non-M pacemakers may prevent E2 clocks from synchronizing with those of the M cells.

Like the strong shared synaptic targets of E1 LNds, the majority of E2 strong output targets do not synapse onto identified clock neurons. But, in contrast to E1, the minority of E2 targets that do form strong connections with identified clock neurons do so more broadly than clock

recurrent E1 targets, forming strong synaptic connections onto the M group, E2, and the LPNs (Figure 8E). Though not as numerous as the synaptic partners of E1, E2 forms many more synaptic connections than either M or E3, and together E1 and E2 make up the bulk of synaptic output from the LN classes (Figure 4C and Supplemental Table S2). Thus, there appear to be two major circadian output conduits from the LN clock neurons within the hemibrain volume, one of which is tightly coupled to the M group and the other whose output is likely more strongly shaped by other clock neuron classes (26).

The E3 group is characterized by a pattern of strong synaptic output that is distinct from E1 and E2 and is synaptically isolated from other identified clock neurons.

The E3 LNds are distinct from the E1 and E2 groups, in that they form approximately half the number synaptic connections (Figure 4C). While clearly distinct from E1 and E2, the E3 group displays some similarity to the M group with respect to its connectivity to identified clock neurons in the hemibrain, forming very few connections with other clock classes while being interconnected by medium strength connections (Figure 1C). Among the identified clock neurons in the hemibrain, the strong output targets of E3 make strong reciprocal connections back to E3, but not to other identified clock neuron classes, though they do form a few medium strength connections onto LPNs (Figure 9E). This sets E3 clearly apart from the other LN groups, all of which have strong synaptic targets that form strong synapses onto other clock neuron classes (Compare Figures 6E, 7E, 8E, and 9E). Thus, the E3 group appears to be uniquely isolated from other identified clock neuron classes with regard to both direct and indirect synaptic connectivity.

The E3 group is unique among the LN clock neurons by virtue of its lacking CRY and PdfR expression (40, 53) and is therefore thought to be relatively isolated from both light/dark cycles

(54) and PDF released from the LNvs. Indeed, the E3 group entrains its molecular clocks more readily to environmental temperature cycles than to light cycles (54) and does not synchronize with PDF expressing LNvs with slowed clocks (26). A close examination of E3 output pathways and the extent to which they converge or fail to converge on endocrine, sleep, and pre-motor centers will offer important insights into how light and temperature are integrated by the circadian system to entrain to environmental cycles of both light and temperature, the latter of which lag behind the former in natural environments.

Neurons without endogenous molecular clocks are likely integral to the central circadian pacemaker network.

The LN clock neuron classes are critical nodes of circadian timekeeping and are predicted to communicate directly with endocrine, sleep, and pre-motor centers to drive circadian outputs (10, 41) and with other clock neuron classes to coordinate network timekeeping (Reviewed by (11)). Thus, the LN classes are assumed to synapse upon other clock neurons to promote an endogenous sense of time and upon non-clock neurons to mediate daily changes in physiology and behavior. Our analysis reveals the presence of a third type of LN clock output target, neurons that mediate connections between identified clock neurons (e.g., Figure 10B and C).

All four functional classes of LN (M, E1, E2, and E3) provide strong synaptic outputs onto neurons that, in turn, form strong synaptic connections onto identified clock neurons within the hemibrain volume (Figures 6E and F, 7E, 8E, and 9E). In the case of E1 and E3 much of the strong output recurring to the clock neuron network is reciprocal. For example, the strong targets of E1 outputs preferentially form strong connections back onto E1 LNds (Figure 7E). For all four groups of LN, strong outputs recurring to the clock network form either strong or medium

strength synapses on the LPNs, implicating this class as a particularly rich hub for polysynaptic inter-clock connectivity (Figures 6E, 7E, 8E, 9E, and 10C; (13)).

Most of the neurons forming strong but indirect connections between identified clock neurons bear no resemblance to known clock neurons and are unlikely therefore to express the molecular circadian clock (e.g., Figure 10B and C). This finding suggests the need to expand our conception of what constitutes the fly's circadian clock network to include "non-clock" neurons that provide strong synaptic connections between the neurons with endogenous molecular circadian clocks. What role might such "inter-clock-neurons" play within a circadian network? Networks underlying central pattern generators (CPGs) might offer clues.

Many CPG networks consist of neurons both with and without endogenous pacemaking activity (Reviewed by (55)). In such networks, connections between pacemaker neurons and follower neurons profoundly shape the time-course of rhythmic outputs, increase the precision of the central pattern generator, and provide a means for adjusting the phasing of its outputs (e.g., (56-59)). Given the distributed daily phases of neural activity displayed by the various classes of clock neurons (60), one is tempted to view the circadian pace-making network as a central pattern generator, albeit a lumberingly slow one. We hypothesize that the "inter-clock neurons" we've identified here (e.g., Figure 10 B and C) play significant roles in the determination of the circadian system's endogenous period, precision, and phasing of rhythmic outputs, much like the follower neurons of central pattern generators described above.

This testable hypothesis is just one of many that emerge from the comprehensive view of clock connectomics afforded by the hemibrain data set (15). This remarkable picture of the synaptic

connectivity displayed by clock neurons identified in this data set (Supplemental Tables 1 and 2), in conjunction with the open-source neuro-informatic resources available to the field (e.g., (16)) and the highly specific genetic tools available for the manipulation of identified neurons (e.g., (61)), will be the basis of a great deal of future work on the neural basis of circadian entrainment, timekeeping, and output.

Methods

Connectome Data and Neuron Identification

All of the data analyzed in this study come from the Hemibrain v1.2.1 dataset made publicly available by Janelia Research Campus (15). The data details a full connectome derived from EM sections of a significant portion of the right hemisphere of a female *Drosophila* brain and small portions of the left hemisphere. These data were collected from a wild type female brain reared under a 12-hour light, 12-hour dark cycle. The specimen was dissected at 5 days of age, 1.5 hours after lights-on (15, 62).

Hemibrain data was accessed via neuPrint and Fly Brain Observatory. Visualization of morphological data was done in the Fly Brain Observatory web interface (NeuroNLP.Hemibrain) while the retrieval of connectome data was done with the Neuprint python package (https://github.com/connectome-neuprint/neuprint-python). Analyses were aided by the use of the pandas (https://pandas.pydata.org/), seaborn (https://seaborn.pydata.org/), and superVenn (https://github.com/gecko984/supervenn) python packages.

Each neuron in the database has a unique bodyID number and may also be identified with a cell-type name based on the name it was given in the literature or on its location and anatomy.

Clock neurons were identified in the database from queries based on their known cell-type names. This means that there may be clock neurons that have been traced in the hemibrain, but if Janelia had not labeled them with their known cell name within the annotation, we have not included them as clock neurons here. The bodyID numbers for identified clock neurons were collected and used in the connectivity analyses to ensure consistency between platforms and future annotations.

The full table of clock neurons, their unique body IDs, and their sequential labels are provided below. The hemibrain annotation does not sequentially label instances of the same cell type. The Fly Brain Observatory does sequentially label cell type instances, however, there is no guarantee that the sequential labeling will consistently correspond to the specific body IDs. Thus, we employed a sequential labeling on a single retrieval from FBO and have used this labeling consistently throughout the paper (Table 1).

Table 1: Identification of Clock Neurons within the Hemibrain Volume

bodyId	type	Sequential label	subphase
2068801704	s-LNv	s-LNv1	M
1664980698	s-LNv	s-LNv2	M
2007068523	s-LNv	s-LNv3	M
1975347348	s-LNv	s-LNv4	M
5813056917	LNd	LNd4	E1
5813021192	LNd	LNd5	E1
5813069648	LNd	LNd6	E2
511051477	5th s-LNv	5th s-LNv	E2
296544364	LNd	LNd1	E3
448260940	LNd	LNd2	E3
5813064789	LNd	LNd3	E3
356818551	LPN	LPN1	

480029788	LPN	LPN2	
450034902	LPN	LPN3	
546977514	LPN	LPN4	
264083994	DN1a	DN1a1	
5813022274	DN1a	DN1a2	
5813010153	DN1pA	DN1pA1	
324846570	DN1pA	DN1pA2	
325529237	DN1pA	DN1pA3	
387944118	DN1pA	DN1pA4	
387166379	DN1pA	DN1pA5	
386834269	DN1pB	DN1pB1	
5813071319	DN1pB	DN1pB2	
1884625521	l-LNv	lLNv1	
2065745704	l-LNv	lLNv2	
5813001741	l-LNv	lLNv3	
5813026773	l-LNv	lLNv4	

Morphological Data Visualization with FlyBrainLab

FlyBrainLab (16) is available as a python environment and a user-friendly web interface. The platform displays the hemibrain EM data and enables the analysis of the connectome data. The morphology images in our paper were generated in FlyBrainLab.

Connectivity Analysis

Synaptic connectivity data were retrieved from the Janelia hemibrain dataset. Our analyses included the synapses to or from traced but unnamed fragments as well as select orphan bodies, in addition to synapses from full, traced, and named neurons. Fragments are partial or truncated neurons that mainly lie beyond or at the boundaries of the hemibrain section. Although fragments were often unidentified cell types, we felt their inclusion was warranted to

obtain as accurate a picture as possible of the relative amounts of synaptic connectivity to and from clock neurons.

In keeping with Scheffer and colleagues (15), the synaptic strengths reported in our paper correspond to the number of postsynaptic densities counted on the postsynaptic neuron that are abutted by the presynaptic T-bar sites from the presynaptic neuron in question. Polyadic synapses, where a single presynaptic T-bar site contacts multiple postsynaptic sites, are common in the Drosophila brain (15, 62). Thus, synaptic weight for both the presynaptic and postsynaptic neuron is quantified as the postsynaptic density count.

We adopted the criteria from Scheffer *et. al* (15) to categorize connectivity strength. A weak connection is defined as a synaptic connection weight less than three. A medium strength connection is between three and nine synapses, while a strong connection is a strength equal to or greater than ten synapses. In our study, these criteria are applied to the total synapse count (i.e. the total number of postsynaptic densities) between two neurons rather than to the per-ROI synapse counts between them. Wherever applicable, the connection strength criteria used for any analysis or visualization is stated in the figure legend and in the main text.

The Sankey figures are based only on strong synaptic connections. Connectivity data were retrieved using the criteria for strong connections and exported into tables. The data was visualized on sankeymatic.com and subsequently edited in Adobe Illustrator for aesthetics and clarity. The network structure of the clock connectome was graphed using the synaptic connectivity data retrieved from the hemibrain data and the networkX python package (https://networkx.org). Nodes are individual clock neurons and edges are labeled with the total synaptic connection weights from one neuron to another.

Jaccard Indices

The Jaccard similarity coefficient is defined as the ratio of the intersection and the union of two sets.

$$J(A,B) = \frac{A \cap B}{A \cup B}$$

In the context of our study the Jaccard index represents the amount of overlap among the synaptic partners of two neurons. The Jaccard index is a number between 0 and 1, with 0 indicating no overlap and with 1 indicating that the sets of synaptic partners for two neurons are identical.

Availability of Analysis Code

The data retrieval routines and the analyses used in this paper were done in the python coding language. We have made our scripts publicly available upon request in a GitHub repository.

Acknowledgements:

This work was supported by grants from the National Institute of Neurological Disorders and Stroke R01NS077933 to O.T.S. and R01NS118012 to M.P.F. and O.T.S., start-up funds from Barnard College (M.P.F.) and the State of New York (O.T.S.), grants NIH K22 NS104187, NSF NeuroNex Award DBI-1707398, and The Gatsby Charitable Foundation to G.J.G, and Barnard SRI funds to K.L and A.M. We are grateful to Michael Rosbash and Annika Barber for helpful discussions and to Aishwarya Ramakrishnan, Abhilash Lakshman and Robert Veline for comments on the manuscript. Figure 1A was created in Biorender.

Figure Legends:

Main Figures

Figure 1. The circadian clock neuron network and identified clock neurons in the hemibrain. (A) The circadian clock network is shown in both hemispheres. Currently identified cells are shown in color (s-LNvs red, l-LNvs light red, LNds in orange, DN1a in purple, a subset of DN1p in blue) and known clock cells not yet identified within the hemibrain connectome data are shown in gray (DN2, DN3, and a subset of DN1p). The *pars intercerebralis* (PI) and optic lobe (OL) are indicated in gray. (B) Identified clock neurons in the hemibrain. Neuropils are shown in gray. Color codes as indicated in (A). (C) Heatmap indicates synaptic connections strength among all identified circadian clock neurons, including weak (weight <3) connections. (D) The timekeeping lateral neurons that compose the morning (M) and evening (E) Oscillators: s-LNvs (M cells), and 5th s-LNv and LNds (E cells).

Figure 2. Connectivity patterns of the s-LNvs. (A-C). Synaptic connections of the four *pdf*+ s-LNvs, s-LNv_R_1 through s-LNv_R_4. Neuronal morphology is shown in gray. In A and B, inputs to the s-LNvs are shown in blue, outputs are shown in magenta. (A) All connections, including non-clock cells, (B) Connections to/from clock cells only, excluding connections to s-LNvs, (C) Connections among the 4 *pdf*+ s-LNvs. Input and output sides coincide and are indicated in green. (D-E) Sankey diagram indicating the strong synaptic partners of all s-LNvs, including the 5th s-LNv. The total weight of synapses formed by each cell with its inputs (D) or outputs (E) is shown. (D) Presynaptic partners (inputs) of s-LNvs. No shared connections were found between the pdf+ s-LNvs and the 5th s-LNv. (E) Post synaptic partners (outputs) of s-LNvs. Only one cell (Body ID 571372889) receives synaptic input from the 5th s-LNv plus a *pdf*+ s-LNv. (F-G) Synaptic connections of the 5th s-LNv. (F) All connections, including non-clock cells, (G) Connections to clock cells only. (H) Connectivity map of the four *pdf*+ s-LNvs.

Figure 3. Connectivity patterns of the LNds. (A-C). Synaptic connections of the six LNds. Neuronal morphology is shown in gray. In A and B, inputs to the s-LNvs are shown in blue, outputs are shown in magenta. (A) All connections, including non-clock cells, (B) Connections to clock cells only, excluding connections to LNds. Input and output sides coincide and are indicated in green. (C) Connections within LNds. (D) Connectivity map of the six LNds. (E-F) Sankey diagram indicating the strong synaptic partners of all LNds. The total weight of synapses formed by each cell with its inputs (E) or outputs (F) is shown. (E) Pre-synaptic partners of LNds. No shared connections were found between LNd1-3 and LNd4-6. Most of the shared connections are between LNd4 and LNd5 (X cells provide strong inputs to both). (F) Post synaptic partners of the LNds.

Figure 4. E cells can be clustered in three distinct groups. (A-B) Jaccard indices for overlap in synaptic partners of M and E cells. Only includes synaptic partners that make medium or strong connections. Higher index values indicate more similarity in either inputs (A) or outputs (B). (C) Total input and output Synapse counts for M and E cells. (D-E) Strong shared connections of the four *pdf*+ s-LNvs. Only cells that share one connection with at least two M cells are shown. The strength (weight) of the connection is indicated. Only medium and strong connections are included. (D) The two cells that send strong connections to at least two M cells send strong connections to all 4. (E) The six cells that receive strong connections from at least two M cells receive strong connections from all 4. (F-G) Strong shared connections of the six LNds plus the 5th s-LNv (collectively referred to as E cells). Only cells that share a strong connection with at least two E cells are shown. The strength (weight) of the connection is indicated. Only medium and strong connections are included. (F) Cells that send strong connections to at least two E cells are included in the heatmap. (G) Cells that receive strong connections from at least two E cells are included in the heatmap.

Figure 5. Neuropils innervated by M and E cells. (A-B). Percentage of connections located in each of the indicated neuropils. Medium and strong connections are included. (A) Neuropils in which the outputs of each of the 4 *pdf*+ s-LNvs are located. (B) Neuropils in which the outputs of each of the LNds and the 5th s-LNv are located.

Figure 6. Strong shared outputs of M cells. (A-C) The six cells that are strong shared outputs of the four M cells involve three different neuronal types (SPL316-R, SLP403-R, and SMP232-R). The M cells outputs onto each representative neuron of each type are shown in magenta. Representative target neurons are shown in green. (A) M cells contact three SPL316 neurons. Left, all four M cells are shown in gray and their contacts to 355453590 (neuronal morphology shown in green) are shown in magenta. Right: 355453590 is shown in gray and its outputs to clock cells are shown in magenta. (A) M cells contact three SPL316 neurons. Left, all four M cells are shown in gray and their contacts to 355453590 (neuronal morphology shown in green) are shown in magenta. Right: 355453590 is shown in gray and its outputs to clock cells are shown in magenta. (B) M cells contact two SPL403-R neurons. Left, all four M cells are shown in gray and their contacts to 325455002 (neuronal morphology shown in green) are shown in magenta. Right: 325455002 is shown in gray and its outputs to clock cells are shown in magenta. (C) M cells contact one SMP232-R neuron. Left, all four M cells are shown in gray and their contacts to 325455002 (neuronal morphology shown in green) are shown in magenta. Right: 325455002 is shown in gray and its outputs to clock cells are shown in magenta. (D) Jaccard index of the six M cell shared output cells. The index is based on the similarity of their outputs, the more similar their outputs are the higher the index value. Y and x-axis indicate the cell body ID of each of the six cells. Their neuronal type is indicated to the left of the body ID on the y axis. Only indices >=0.01 are shown. (E) All strong shared outputs of M cells in turn contact clock neurons. On the x-axis, the clock neurons that receive contacts from each cell are indicated. The values on the cells represent the weight of each connection. Medium and strong connections are included. (F) Percent of strong shared outputs of each neuronal class that in turn sends contacts to clock cells. Medium and strong connections are included. E1 = LNd4 and LNd5, E2 = LNd6 and the 5th s-LNv, E3= LNd1, LNd2 and LNd3.

Figure 7. Strong shared outputs of E1. (A-C) The cells that are strong shared outputs of E1 involve multiple neuronal types. E1 outputs onto three representative neurons are shown. E1 neurons (LNd4 and LNd5) are shown in gray in the left panels, where representative output neurons are shown in green. On the right panels, each representative cell is shown in gray and its contacts to clock cells are shown in magenta (A) E1 cells contact two SMP368-R neurons. Left, E1 neurons (shown in gray) contacts to SMP368-R neuron 390331583 (shown in green) are shown in magenta. (B) E1 cells contact two AVLP075-R neurons. Left, E1 neurons (shown in gray) contacts to AVLP075-R neuron 702152113 (shown in green) are shown in magenta. (C) E1 cells contact two SMP315-R neurons. Left, E1 neurons (shown in gray) contacts to SMP315-R neuron 5813040712 (shown in green) are shown in magenta. (D) Jaccard indices indicating overlap among the output synaptic partners of the top 10 E1 strong shared output cells. The index is based on the similarity of their outputs, the more similar their outputs are the higher the index value. Y and x-axis indicate the cell body ID of each of the six cells. Only indices >=0.01 are shown. (E) Most shared outputs of E1 cells that contact clock cells send strong contacts to both E1 neurons. On the x-axis, the clock neurons that receive contacts from each cell are indicated. The values on the cells represent the weight of each connection. Medium and strong connections are included.

Figure 8. Strong shared outputs of E2. (A-C) The cells that are strong shared outputs of E2 involve multiple neuronal types. E2 outputs onto three representative neurons are shown. E2 neurons (LNd6 and the 5th s-LNv) are shown in gray in the left panels, where representative output neurons are shown in green. On the right panels, each representative cell is shown in gray and its contacts to clock cells are shown in magenta (A) Left, E2 neurons (shown in gray) contacts to SMP368 neuron 329732855 (shown in green) are shown in magenta. (B) Left, E2 neurons (shown in gray) contacts to SLP249 neuron 356140100 (shown in green) are shown in magenta. (C) Left, E2 neurons (shown in gray) contacts to aMe22 neuron 5813021192 (shown in green) are shown in magenta. (D) Jaccard indices for the outputs of the top 10 E2 strong shared output cells. The index is based on the similarity of their outputs, the more similar their outputs are the higher the index value. Y and x-axis indicate the cell body ID of each of the ten cells. One of the strong shared outputs of E2 is LNd4. Only indices >=0.01 are shown. (E) Shared outputs of E2 that contact clock cells contact different clock subclasses. On the x-axis, the clock neurons that receive contacts from each cell are indicated. The values on the cells represent the weight of each connection. Medium and strong connections are included.

Figure 9. Strong shared outputs of E3. (A-C) The cells that are strong shared outputs of E3 involve multiple neuronal types. E3 outputs onto three representative neurons are shown. E3 neurons (LNd1, LNd2, and LNd3) are shown in gray in the left panels, where representative output neurons are shown in green. On the right panels, each representative cell is shown in gray and its contacts to clock cells are shown in magenta (A) Left, E3 neurons (shown in gray) contacts to SMP335 neuron 297243542 (shown in green) are shown in magenta. (B) Left, E3 neurons (shown in gray) contacts to SMP486 neuron 327933679 (shown in green) are shown in magenta. (C) Left, E3 neurons (shown in gray) contacts to SMP334 neuron 360254108 (shown in green) are shown in magenta. (D) Jaccard indices for the outputs of the top 11 E3 strong

shared output cells. The index is based on the similarity of their outputs, the more similar their outputs are the higher the index value. Y and x-axis indicate the cell body ID of each of the cells. Only 3 cells are strong shared outputs of all E3 cells (E3a+ E3b). 8 cells are strong shared targets of E3a only. Only indices >=0.01 are shown. (E) Shared outputs of any two E3 cells that contact clock cells. On the x-axis, the clock neurons that receive contacts from each cell are indicated. The values on the cells represent the weight of each connection. Medium and strong connections are included.

Figure 10. Connections within the clock neuron network. (A) Combined weights of medium and strong connections among different classes of identified clock neurons. Arrows indicate the direction of the connection. Some classes, such as E2, are strongly interconnected, while other clusters are relatively isolated. (B) Representative strong shared output of E1 that in turn contacts clock neurons. E1 are indicated in gray, their strong shared target LHPV6m1 cell 388881226 is indicated in green, and its strong target neurons DNa1 and 2 are indicated in magenta (the weight of output contacts is 19 and 10, respectively). (C) Representative strong shared output of E2 that in turn contacts clock neurons. E2 are indicated in gray, their strong shared target SMP223 cell 417143726 is indicated in green, and its strong target neurons LPN are indicated in magenta (the weight of output contacts is 14 to LPN, 18 to LPN2, and 20 to LPN3).

Supplementary Figures

Supplementary Figure 1. Connections of individual s-LNvs. (A-D). Synaptic connections of each of the four *pdf*+ s-LNvs, s-LNv1 (A), s-LNv2 (B), s-LNv3 (C) and s-LNv4 (D), either to all neurons (left columns), to other clock cells except s-LNvs (middle columns), or to other s-LNvs (right columns). Neuronal morphology is shown in gray. Inputs to the s-LNvs are shown in blue, outputs are shown in magenta. Body IDs of each s-LNv are indicated on the right.

Supplementary Figure 2. Connections of individual LNds. (A-F). Synaptic connections of each of the six LNds, LNd1 (A), LNd2 (B), LNd3 (C), LNd4 (D), LNd5 (E) and LNd6 (F) either to all neurons (left columns), to other clock cells except LNds (middle columns), or to other LNds (right columns). Neuronal morphology is shown in gray. Inputs to the LNds are shown in blue, outputs of the LNds are shown in magenta. Body IDs of each LNd are indicated on the right.

Supplementary Figure 3. Connections of E cell classes. (A-C). Synaptic connections of the three E cell classes, E3a (A), E1 (B), and E2 (C) either to all neurons (left columns), to other clock cells except LNds (middle columns), or to other LNds (right columns). LNd1 alone (E3b) is shown in Suppl. Figure 2A. Neuronal morphology is shown in gray. Inputs to the E classes are shown in blue, outputs are shown in magenta (left and middle columns). Within each group (right columns), input and output sides coincide and are indicated in green.

Supplementary Figure 4. Comparison of medium and strong inputs of 5th s-LNv relative to the *pdf*+ s-LNvs and the LNds. (A-B) Supervenn diagrams indicate the number of shared

inputs between all combinations of neurons, either among the 5th s-LNv and the LNds (A) or among the 5th s-LNv and the *pdf*+ s-LNvs (B). Each neuron is represented in a row, boxes in color indicate inputs to that neuron. The numbers on the right y-axis indicate the total number of neurons that provide input to that cell. For example, 74 neurons provide medium and strong inputs to LNd3. The numbers on the x-axis indicate the number of shared inputs between different combinations of cells.

Supplementary Figure 5. Comparison of medium and strong outputs of 5th s-LNv relative to the *pdf*+ s-LNvs and the LNds. (A-B) Supervenn diagrams indicate the number of shared outputs between all combinations of neurons, either among the 5th s-LNv and the LNds (A) or among the 5th s-LNv and the *pdf*+ s-LNvs (B). Each neuron is represented in a row, boxes in color indicate inputs to that neuron. The numbers on the right y-axis indicate the total number of neurons that are being contacted by a specific cell. For example, 172 neurons receive medium or strong contacts from LNd3. The numbers on the x-axis indicate the number of shared outputs between different combinations of cells.

Supplementary Figure 6. Connections of individual strong shared outputs of s-LNvs. (A-F). Synaptic connections of each of the six cells that receive strong shared inputs from all four *pdf*+ s-LNvs. Each cell is indicated in gray. Inputs from clock neurons to each cell are indicated in blue, and outputs from each cell to any clock neurons are indicated in magenta. (A-C) Three SLP316 receive the strongest contacts from all *pdf*+ s-LNvs and are indicated in gray. (D-E) Two SLP403 are indicated in gray. (F) SMP223 is indicated in gray.

Supplementary Figure 7. Neuroanatomy of the three SLP316 cells and identified DN1s. (A) Five DN1ps (green) that exhibit contralateral as well as dorsal projections have been identified, and are referred to as DN1pA. (B) Two DN1ps (magenta) that lack a contralateral or dorsal projection but extend ventrally and medially have been identified and are referred to as DN1pB. (C) The three SPL316 neurons (gray) have both dorsal and ventral projections and a short medial projection. (D) Overlap of DN1pA, DN1pB, and SLP316.

References

1. J. Aschoff, *Handbook of behavioral neurobiology, biological rhythms* (Plenum Press, New York, ed. 4, 1981).
2. J. S. Takahashi, Turek, F.W., Moore, R.Y., *Biological Rhythms*, Handbook of Behavioral Neurobiology (Plenum Press, New York, ed. 12, 2001).
3. E. D. Herzog, Neurons and networks in daily rhythms. *Nat Rev Neurosci* **8**, 790-802 (2007).
4. E. D. Herzog, T. Hermanstyne, N. J. Smyllie, M. H. Hastings, Regulating the Suprachiasmatic Nucleus (SCN) Circadian Clockwork: Interplay between Cell-Autonomous and Circuit-Level Mechanisms. *Cold Spring Harb Perspect Biol* **9** (2017).
5. A. C. Liu *et al.*, Intercellular coupling confers robustness against mutations in the SCN circadian clock network. *Cell* **129**, 605-616 (2007).

6. E. D. Buhr, S. H. Yoo, J. S. Takahashi, Temperature as a universal resetting cue for mammalian circadian oscillators. *Science* **330**, 379-385 (2010).
7. M. H. Hastings, E. S. Maywood, M. Brancaccio, The Mammalian Circadian Timing System and the Suprachiasmatic Nucleus as Its Pacemaker. *Biology (Basel)* **8** (2019).
8. M. N. Nitabach, P. H. Taghert, Organization of the Drosophila circadian control circuit. *Curr Biol* **18**, R84-93 (2008).
9. O. T. Shafer, C. Helfrich-Forster, S. C. Renn, P. H. Taghert, Reevaluation of Drosophila melanogaster's neuronal circadian pacemakers reveals new neuronal classes. *J Comp Neurol* **498**, 180-193 (2006).
10. O. T. Shafer, A. C. Keene, The Regulation of Drosophila Sleep. *Curr Biol* **31**, R38-R49 (2021).
11. M. Ahmad, W. Li, D. Top, Integration of Circadian Clock Information in the Drosophila Circadian Neuronal Network. *J Biol Rhythms* **36**, 203-220 (2021).
12. Z. Yao, A. M. Macara, K. R. Lelito, T. Y. Minosyan, O. T. Shafer, Analysis of functional neuronal connectivity in the Drosophila brain. *Journal of neurophysiology* **108**, 684-696 (2012).
13. N. Reinhard *et al.*, The lateral posterior clock neurons of Drosophila melanogaster express three neuropeptides and have multiple connections within the circadian clock network and beyond. *J Comp Neurol* 10.1002/cne.25294 (2021).
14. N. Kasthuri *et al.*, Saturated Reconstruction of a Volume of Neocortex. *Cell* **162**, 648-661 (2015).
15. L. K. Scheffer *et al.*, A connectome and analysis of the adult Drosophila central brain. *Elife* **9** (2020).
16. A. A. Lazar, T. Liu, M. K. Turkcan, Y. Zhou, Accelerating with FlyBrainLab the discovery of the functional logic of the Drosophila brain in the connectomic and synaptomic era. *Elife* **10** (2021).
17. B. Grima, E. Chelot, R. Xia, F. Rouyer, Morning and evening peaks of activity rely on different clock neurons of the Drosophila brain. *Nature* **431**, 869-873 (2004).
18. D. Rieger, O. T. Shafer, K. Tomioka, C. Helfrich-Forster, Functional analysis of circadian pacemaker neurons in Drosophila melanogaster. *J Neurosci* **26**, 2531-2543 (2006).
19. C. Helfrich-Forster, Robust circadian rhythmicity of Drosophila melanogaster requires the presence of lateral neurons: a brain-behavioral study of disconnected mutants. *J Comp Physiol A* **182**, 435-453 (1998).
20. C. Helfrich-Forster, The period clock gene is expressed in central nervous system neurons which also produce a neuropeptide that reveals the projections of circadian pacemaker cells within the brain of Drosophila melanogaster. *Proc Natl Acad Sci U S A* **92**, 612-616 (1995).
21. S. C. Renn, J. H. Park, M. Rosbash, J. C. Hall, P. H. Taghert, A pdf neuropeptide gene mutation and ablation of PDF neurons each cause severe abnormalities of behavioral circadian rhythms in Drosophila. *Cell* **99**, 791-802 (1999).
22. Z. Yang, A. Sehgal, Role of molecular oscillations in generating behavioral rhythms in Drosophila. *Neuron* **29**, 453-467 (2001).
23. O. T. Shafer, M. Rosbash, J. W. Truman, Sequential nuclear accumulation of the clock proteins period and timeless in the pacemaker neurons of Drosophila melanogaster. *J Neurosci* **22**, 5946-5954 (2002).
24. O. T. Shafer, P. H. Taghert, RNA-interference knockdown of Drosophila pigment dispersing factor in neuronal subsets: the anatomical basis of a neuropeptide's circadian functions. *PLoS One* **4**, e8298 (2009).
25. D. Stoleru, Y. Peng, J. Agosto, M. Rosbash, Coupled oscillators control morning and evening locomotor behaviour of Drosophila. *Nature* **431**, 862-868 (2004).

26. Z. Yao, O. T. Shafer, The Drosophila circadian clock is a variably coupled network of multiple peptidergic units. *Science* **343**, 1516-1520 (2014).
27. M. Schlichting, M. M. Diaz, J. Xin, M. Rosbash, Neuron-specific knockouts indicate the importance of network communication to Drosophila rhythmicity. *Elife* **8** (2019).
28. R. Delventhal *et al.*, Dissection of central clock function in Drosophila through cell-specific CRISPR-mediated clock gene disruption. *Elife* **8** (2019).
29. M. Kaneko, J. C. Hall, Neuroanatomy of cells expressing clock genes in Drosophila: transgenic manipulation of the period and timeless genes to mark the perikarya of circadian pacemaker neurons and their projections. *J Comp Neurol* **422**, 66-94 (2000).
30. F. K. Schubert, N. Hagedorn, T. Yoshii, C. Helfrich-Forster, D. Rieger, Neuroanatomical details of the lateral neurons of Drosophila melanogaster support their functional role in the circadian system. *J Comp Neurol* **526**, 1209-1231 (2018).
31. C. Helfrich-Forster *et al.*, Development and morphology of the clock-gene-expressing lateral neurons of Drosophila melanogaster. *J Comp Neurol* **500**, 47-70 (2007).
32. S. Malpel, A. Klarsfeld, F. Rouyer, Larval optic nerve and adult extra-retinal photoreceptors sequentially associate with clock neurons during Drosophila brain development. *Development* **129**, 1443-1453 (2002).
33. C. Helfrich-Forster *et al.*, The extraretinal eyelet of Drosophila: development, ultrastructure, and putative circadian function. *J Neurosci* **22**, 9255-9266 (2002).
34. C. Helfrich-Förster, Development of pigment-dispersing hormone-immunoreactive neurons in the nervous system of Drosophila melanogaster. *Journal of Comparative Neurology* **380**, 335-354 (1997).
35. K. Yasuyama, I. A. Meinertzhagen, Synaptic connections of PDF-immunoreactive lateral neurons projecting to the dorsal protocerebrum of Drosophila melanogaster. *J Comp Neurol* **518**, 292-304 (2010).
36. D. Rieger, R. Stanewsky, C. Helfrich-Forster, Cryptochrome, compound eyes, Hofbauer-Buchner eyelets, and ocelli play different roles in the entrainment and masking pathway of the locomotor activity rhythm in the fruit fly Drosophila melanogaster. *J Biol Rhythms* **18**, 377-391 (2003).
37. M. T. Li *et al.*, Hub-organized parallel circuits of central circadian pacemaker neurons for visual photoentrainment in Drosophila. *Nat Commun* **9**, 4247 (2018).
38. D. Ma *et al.*, A transcriptomic taxonomy of Drosophila circadian neurons around the clock. *Elife* **10** (2021).
39. H. A. D. Johard *et al.*, Peptidergic clock neurons in Drosophila: Ion transport peptide and short neuropeptide F in subsets of dorsal and ventral lateral neurons. *The Journal of Comparative Neurology* **516**, 59-73 (2009).
40. S. H. Im, W. Li, P. H. Taghert, PDFR and CRY signaling converge in a subset of clock neurons to modulate the amplitude and phase of circadian behavior in Drosophila. *PLoS One* **6**, e18974 (2011).
41. A. N. King, A. Sehgal, Molecular and circuit mechanisms mediating circadian clock output in the Drosophila brain. *Eur J Neurosci* **51**, 268-281 (2020).
42. X. Liang *et al.*, Morning and Evening Circadian Pacemakers Independently Drive Premotor Centers via a Specific Dopamine Relay. *Neuron* **102**, 843-857 e844 (2019).
43. F. Guo, M. Holla, M. M. Diaz, M. Rosbash, A Circadian Output Circuit Controls Sleep-Wake Arousal in Drosophila. *Neuron* **100**, 624-635 e624 (2018).
44. A. Lamaze, P. Kratschmer, K. F. Chen, S. Lowe, J. E. C. Jepson, A Wake-Promoting Circadian Output Circuit in Drosophila. *Curr Biol* **28**, 3098-3105 e3093 (2018).
45. C. Helfrich-Forster *et al.*, The lateral and dorsal neurons of Drosophila melanogaster: new insights about their morphology and function. *Cold Spring Harb Symp Quant Biol* **72**, 517-525 (2007).

46. A. Ramakrishnan, V. Sheeba, Gap junction protein Innexin2 modulates the period of free-running rhythms in Drosophila melanogaster. *iScience* **24**, 103011 (2021).
47. M. P. Fernandez, J. Berni, M. F. Ceriani, Circadian remodeling of neuronal circuits involved in rhythmic behavior. *PLoS Biol* **6**, e69 (2008).
48. J. M. Duhart *et al.*, Circadian Structural Plasticity Drives Remodeling of E Cell Output. *Curr Biol* **30**, 5040-5048 e5045 (2020).
49. B. J. Song, S. J. Sharp, D. Rogulja, Daily rewiring of a neural circuit generates a predictive model of environmental light. *Sci Adv* **7** (2021).
50. F. Guo *et al.*, Circadian neuron feedback controls the Drosophila sleep--activity profile. *Nature* **536**, 292-297 (2016).
51. S. Yadlapalli *et al.*, Circadian clock neurons constantly monitor environmental temperature to set sleep timing. *Nature* **555**, 98-102 (2018).
52. M. P. Fernandez *et al.*, Sites of Circadian Clock Neuron Plasticity Mediate Sensory Integration and Entrainment. *Curr Biol* **30**, 2225-2237 e2225 (2020).
53. T. Yoshii, T. Todo, C. Wulbeck, R. Stanewsky, C. Helfrich-Forster, Cryptochrome is present in the compound eyes and a subset of Drosophila's clock neurons. *J Comp Neurol* **508**, 952-966 (2008).
54. T. Yoshii, C. Hermann, C. Helfrich-Forster, Cryptochrome-positive and -negative clock neurons in Drosophila entrain differentially to light and temperature. *J Biol Rhythms* **25**, 387-398 (2010).
55. E. Marder, D. Bucher, D. J. Schulz, A. L. Taylor, Invertebrate central pattern generation moves along. *Curr Biol* **15**, R685-699 (2005).
56. A. I. Selverston, J. P. Miller, Mechanisms underlying pattern generation in lobster stomatogastric ganglion as determined by selective inactivation of identified neurons. I. Pyloric system. *Journal of neurophysiology* **44**, 1102-1121 (1980).
57. A. L. Weaver, R. C. Roffman, B. J. Norris, R. L. Calabrese, A role for compromise: synaptic inhibition and electrical coupling interact to control phasing in the leech heartbeat CpG. *Front Behav Neurosci* **4** (2010).
58. F. Nadim, S. Zhao, L. Zhou, A. Bose, Inhibitory feedback promotes stability in an oscillatory network. *J Neural Eng* **8**, 065001 (2011).
59. L. K. Purvis, T. M. Wright, J. C. Smith, R. J. Butera, Significance of pacemaker vs. non-pacemaker neurons in an excitatory rhythmic network. *Conf Proc IEEE Eng Med Biol Soc* **2006**, 607-608 (2006).
60. X. Liang, T. E. Holy, P. H. Taghert, Synchronous Drosophila circadian pacemakers display nonsynchronous Ca(2)(+) rhythms in vivo. *Science* **351**, 976-981 (2016).
61. H. Dionne, K. L. Hibbard, A. Cavallaro, J. C. Kao, G. M. Rubin, Genetic Reagents for Making Split-GAL4 Lines in Drosophila. *Genetics* **209**, 31-35 (2018).
62. B. K. Hulse *et al.*, A connectome of the Drosophila central complex reveals network motifs suitable for flexible navigation and context-dependent action selection. *Elife* **10** (2021).

Figure 1.

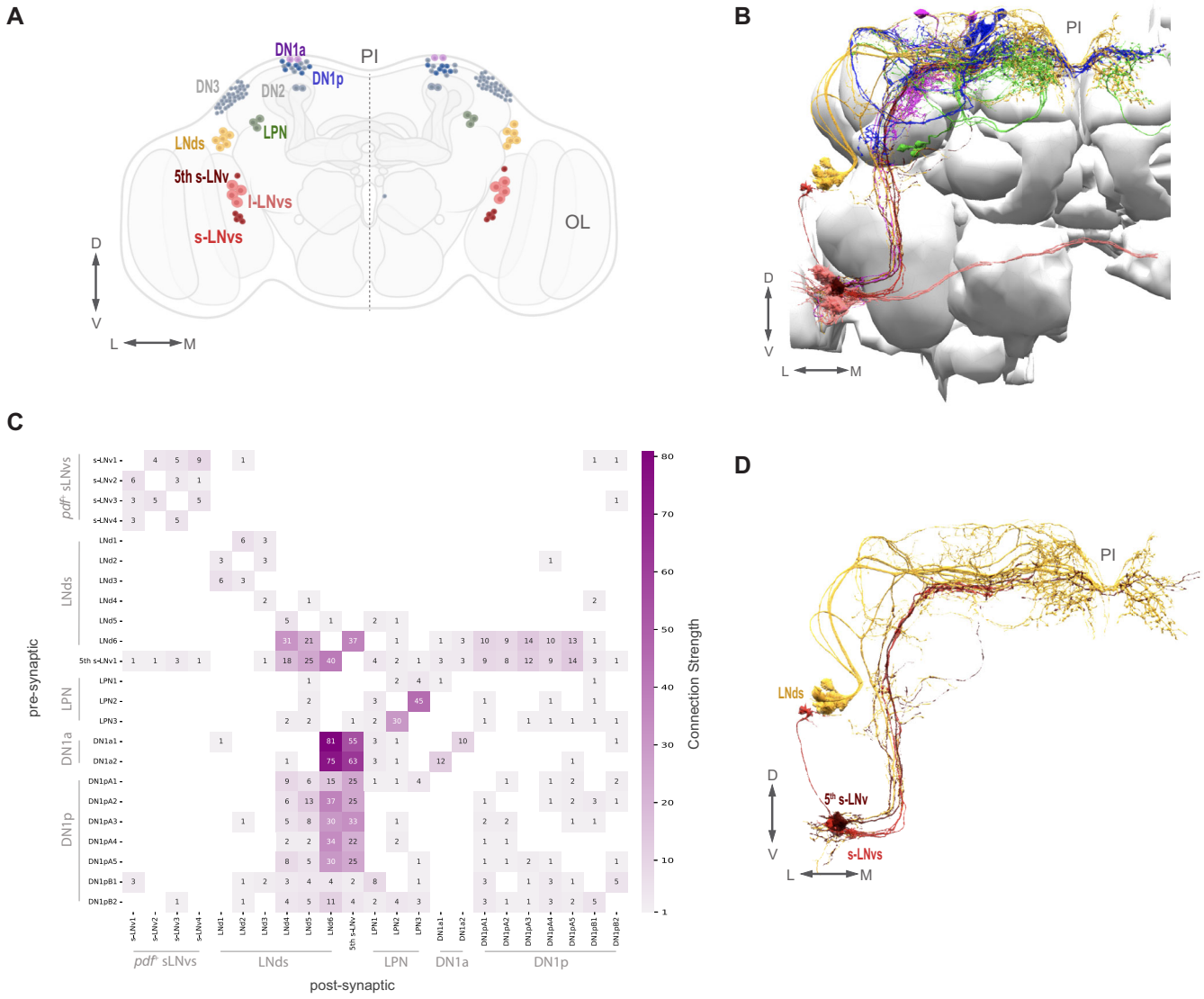

Figure 2.

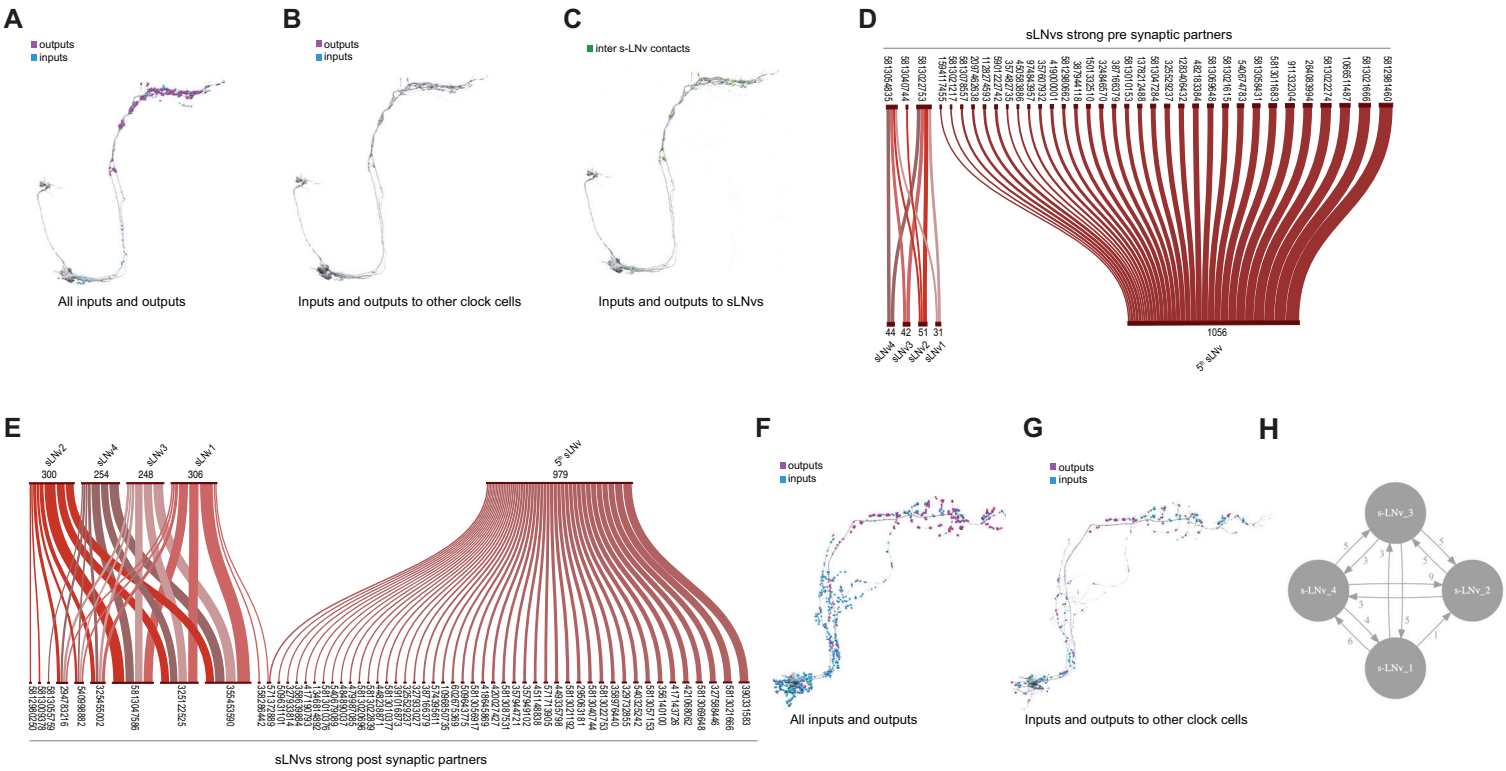

Figure 3.

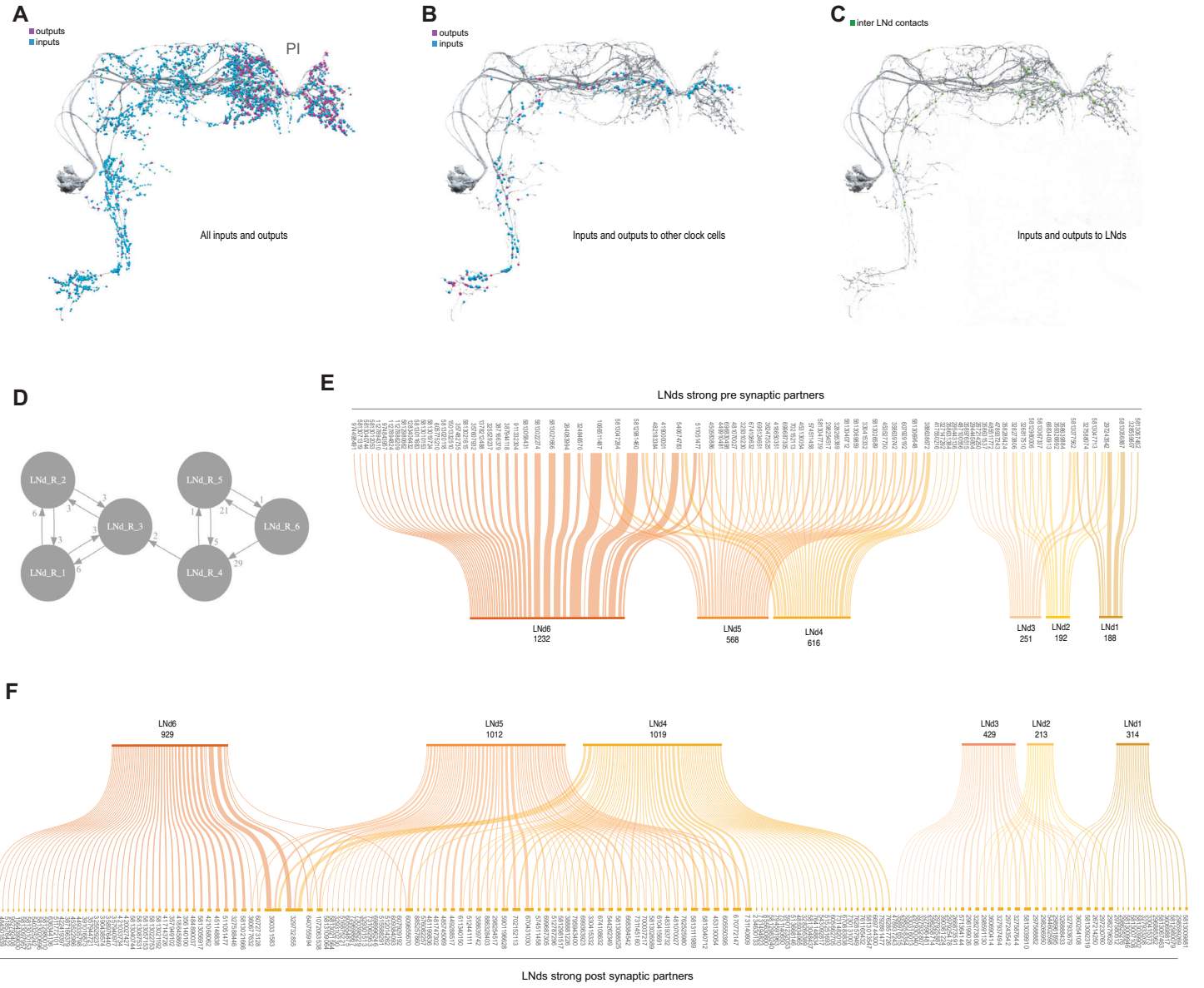

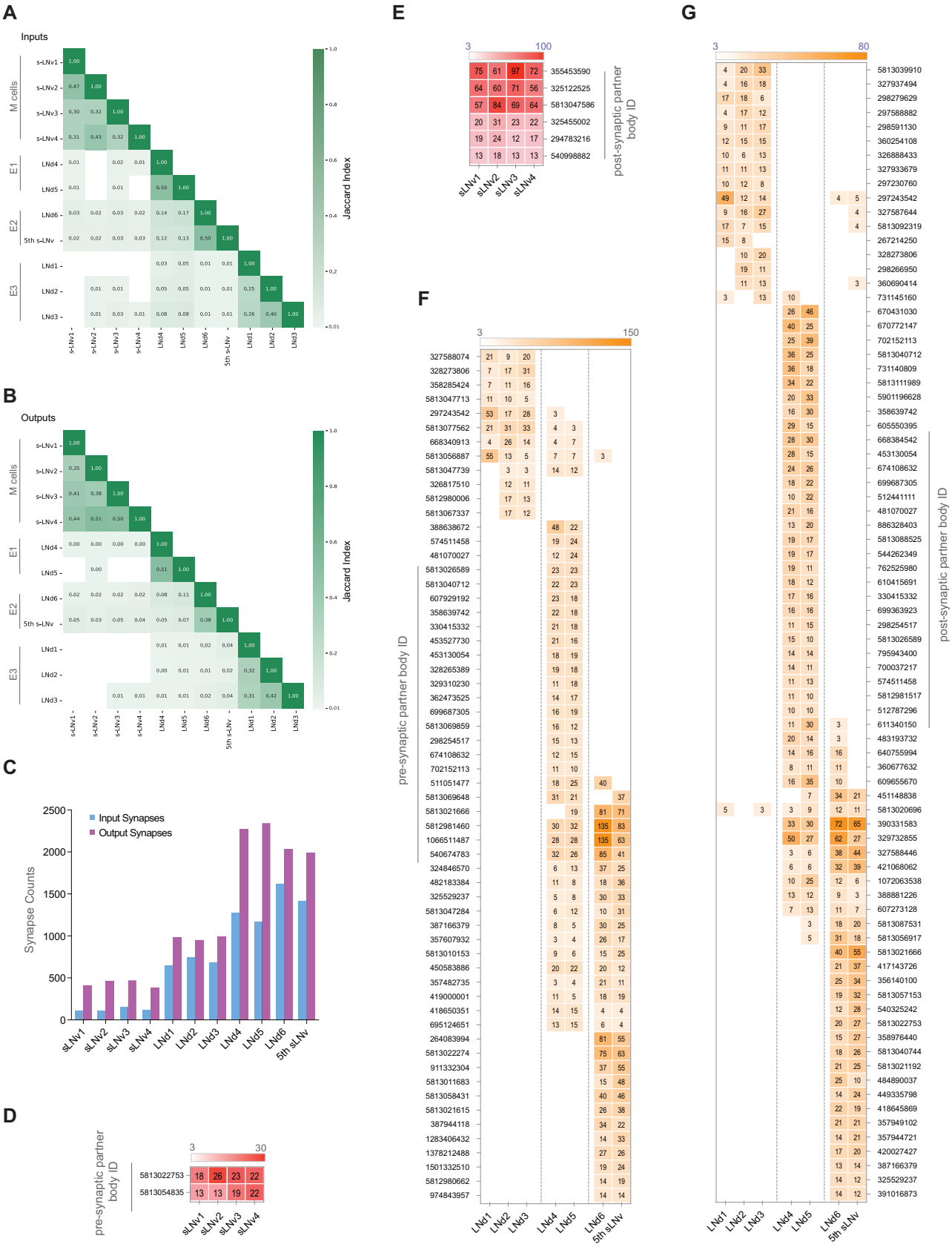

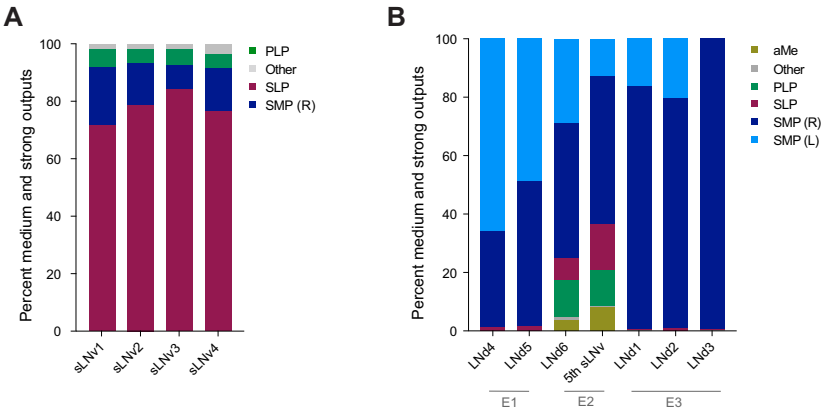

Figure 6

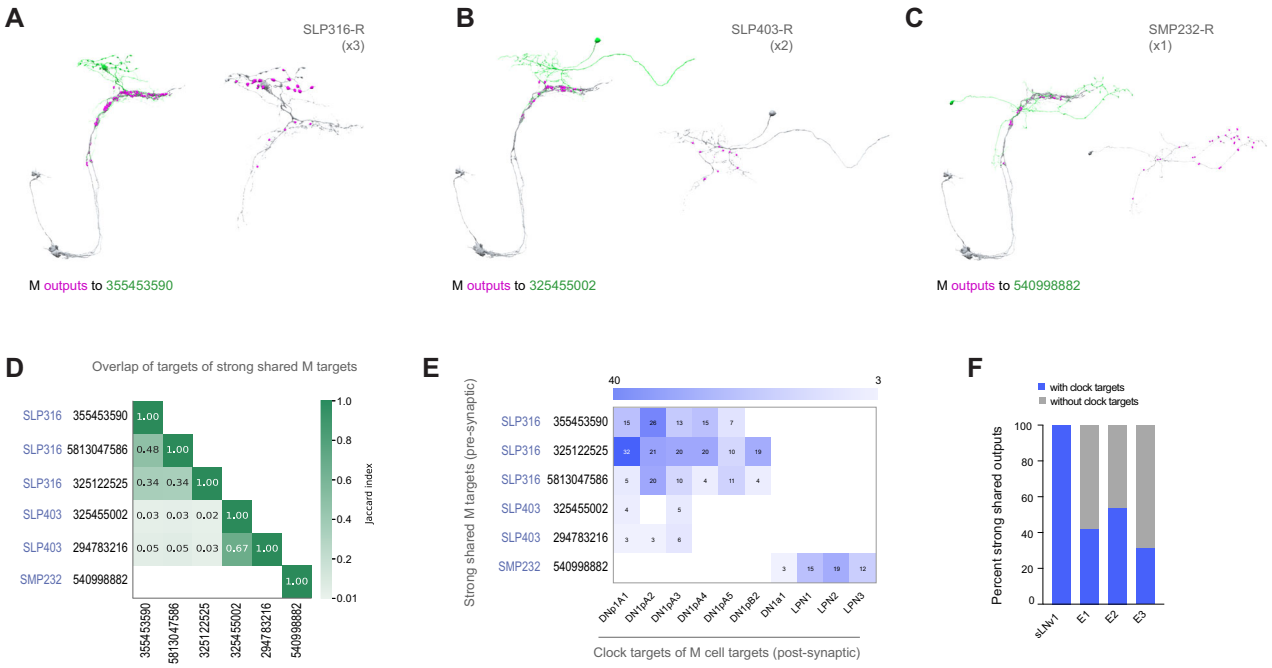

Figure 7

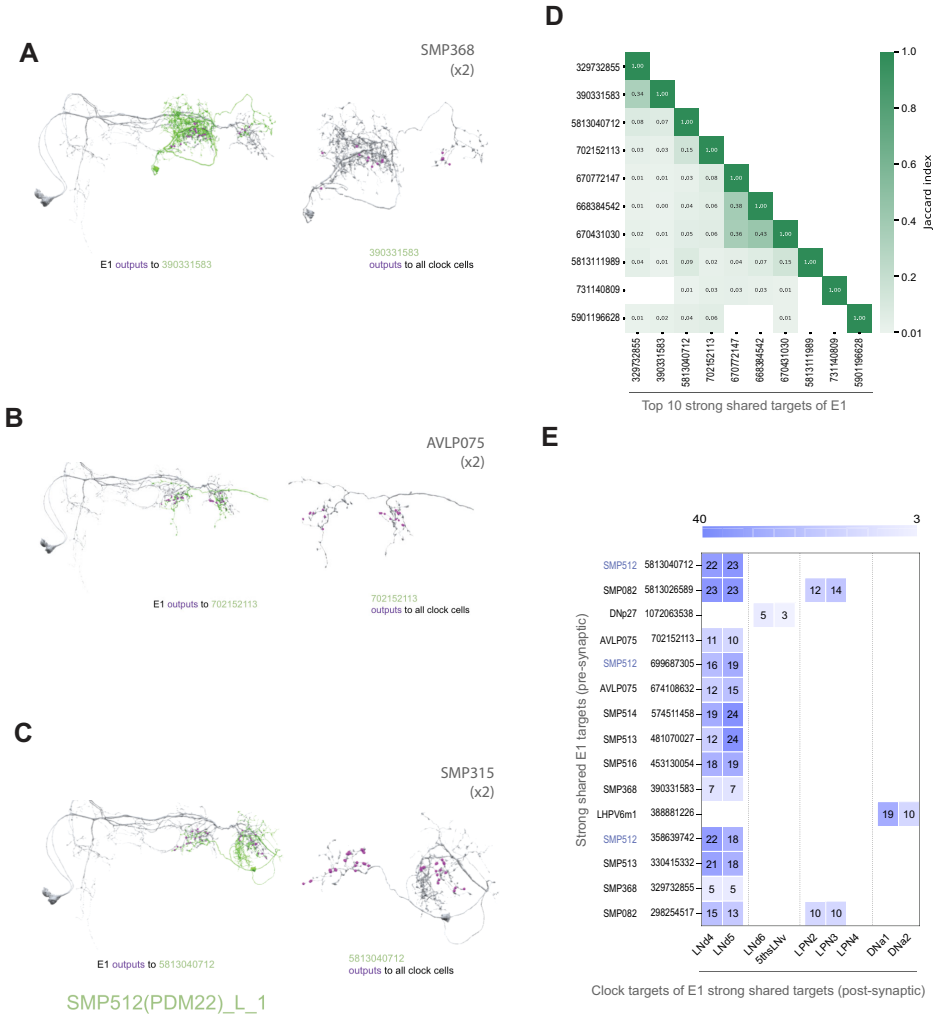

A

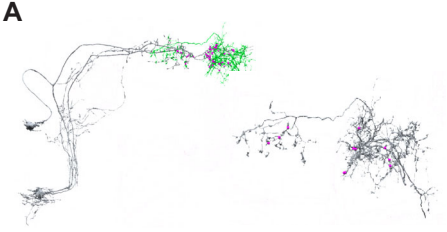

E2 outputs to 329732855

B

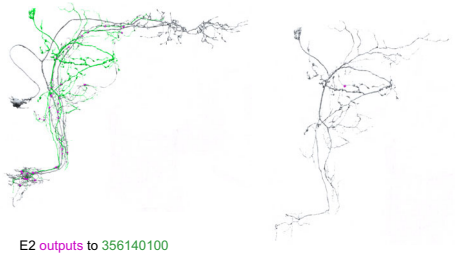

E2 outputs to 356140100

C

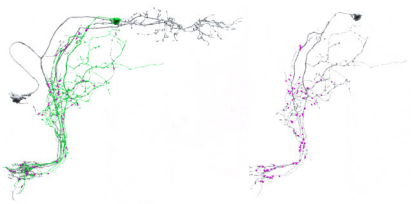

E2 outputs to 5813021666

D

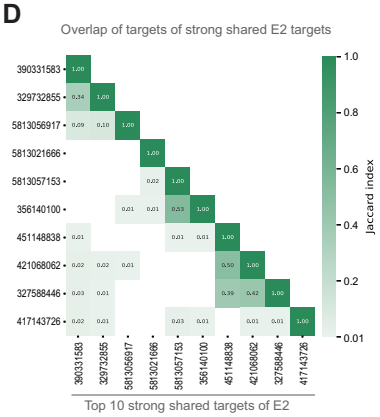

E

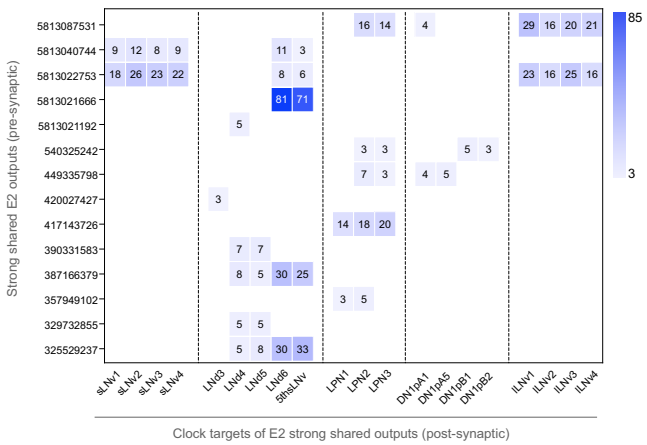

Figure 9.

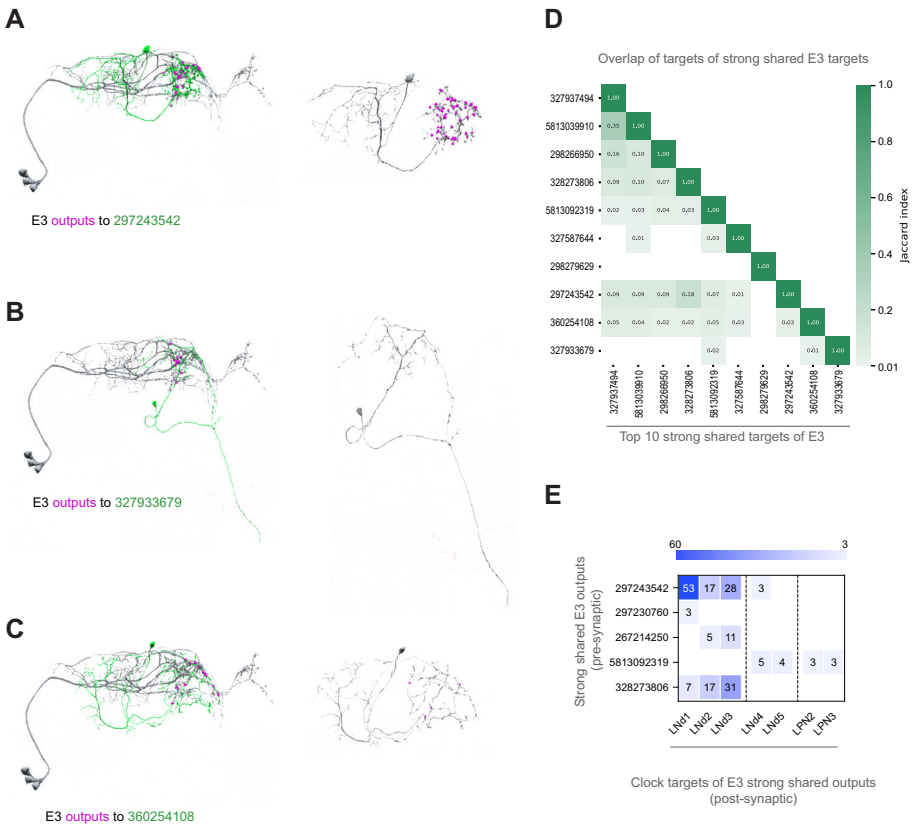

Figure 10